A&A 530, L15 (2011)
DOI: 10.1051/0004-6361/201016258

Astronomy & Astrophysics

Letter to the Editor

Disk and wind kinematics in MWC 349 A

J. Martín-Pintado[1], C. Thum[2], P. Planesas[3], and A. Báez-Rubio[1]

[1] Centro de Astrobiologıa (CSIC-INTA), Ctra de Torrejón a Ajalvir, km 4, 28850 Torrejón de Ardoz, Madrid, Spain
e-mail: jmartin@cab.inta-csic.es
[2] Institut de Radio Astronomie Millimétrique, Domaine Universitaire de Grenoble, 300 Rue de la Piscine, 38406 St. Martin de Héres, France
[3] Joint ALMA Observatory & ESO, Alonso de Cordova 3107, Vitacura, Santiago 7630355, Chile

Received 3 December 2010 / Accepted 30 April 2011

ABSTRACT

Context. Recombination-line maser emission arising from MWC 349 A offers a unique possibility to study the disk kinematics and the origin of ionized outflows driven by massive stars.
Aims. We aim to constrain the disk inclination and its kinematics as well as the main parameters of the outflow launching processes.
Methods. We used the IRAM interferometer to measure the relative positions of the H30α centroid emission as a function of the radial velocity with an accuracy of ~2 mas (2.4 AU) for the strongest maser features and ~5 mas (6 AU) for the weaker line wings.
Results. In addition to the east-west velocity gradient expected for a rotating disk, our data reveal for the first time the complex velocity gradients perpendicular to the disk that are related to the ejection of the ionized gas from the disk.
Conclusions. From the comparison of the data with non-LTE 3D radiative transfer model predictions of the H30α line we conclude that the kinematics in the outer parts of the disk is represented by pure Keplerian rotation. We constrain the wind launching radius to less than 25 AU, much smaller than the gravitational radius of ~150 AU. The ionized outflow seems to be launched from the disk surface because it is rotating in the same sense than the disk. Disk wind models seem to explain the inferred kinematics.

Key words. masers – HII regions – stars: winds, outflows – accretion, accretion disks

1. Introduction

Disks around massive protostars are expected to play a fundamental role in the formation and the evolution of these stars. Recent high angular resolution observations of massive protostars with luminosity $\leq 10^{4.5}$ $L_{\odot}$ have shown that their formation seems to proceed through accretion of material from circumstellar disks (see e.g. Jiménez-Serra et al. 2007). The long lifetime of the ultra-compact HII regions (UC H II) (Churchwell 1990) could be explained if they were formed by photoevaporation of the neutral disk that is left after star formation (Hollenbach et al. 1994). Jaffe & Martín-Pintado (1999) have found that a substantial fraction, ~30%, of UC H II regions show the properties of low velocity ionized winds generated from evaporating disks.

The disk kinematics and the origin of the ionized winds are, so far, unknown. Analytic hydrodynamic models predict that photoevaporation must occur at radii larger than the gravitational radius of the star (Hollenbach et al. 1994). However, simulations indicate that the launching point for the ionized wind has been overestimated in the analytic models by a factor of ~3 (Font et al. 2004). The two classes of magnetically driven wind models, X-winds (Shu et al. 1994) and disk winds (Blandford & Payne 1982), also predict a different location for the outflow launching radius.

MWC 349 A is one of the best examples of a massive protostar surrounded by a photoevaporating disk that produces an ionized outflow expanding at nearly constant velocity (Olnon 1975). The strong radio recombination-line masers detected at mm, submm, far-IR and mid-IR wavelengths in this source (Martín-Pintado et al. 1989; Thum et al. 1994; Strelnitski et al. 1996; Thum et al. 1998) offer a unique opportunity to measure the kinematics of the ionized gas both on the disk surface and in the outflow (Martín-Pintado et al. 1994). Planesas et al. (1992) have used the phase reference technique to show that the centroids of the two H30α maser peaks originate in two positions separated by 0″.065 (78 AU, assuming a distance of 1.2 kpc) in a nearly edge-on, neutral disk. It has been proposed that the disk is in Keplerian rotation around an object with ~30 $M_{\odot}$ (Planesas et al. 1992; Ponomarev et al. 1994). However, the disk around MWC 349 A does not seem to follow a pure Keplerian rotation law (Thum et al. 1994; Weintroub et al. 2008). The kinematics of the ionized wind is also subject of debate. While Rodriguez & Bastian (1994) claimed a complex outflow kinematics with expansion and rotation in the opposite sense of that of the disk, Martín-Pintado et al. (1993) argued for a non-rotating ionized wind.

In this paper[1], we present unprecedented very high-sensitivity observations of the H30α line maser emission toward MWC 349 A, which show for the first time the kinematics of the region where the ionized outflow is launched.

2. Observations and data reduction

We used the IRAM Plateau de Bure interferometer on 15 and 16 January 2005 under very good weather conditions. During our run the precipitable water vapor column was below 2 mm. The 6-element interferometer was in its extended configuration with baselines ranging between 32 and 400 m. The 1.3 mm re-

[1] Based on observations carried out with the IRAM Plateau de Bure Interferometer. IRAM is supported by INSU/CNRS (France), MPG (Germany), and IGN (Spain).

ceivers were tuned to the H30α line at 231.90094 GHz. The receivers were connected to four units of the spectral correlator, which were set up to produce a low- and a high-resolution spectrum centered on each line. The low-resolution H30α spectra have a channel spacing and bandwidth of 3.3 km s^{-1} and 670 km s^{-1} respectively while the high-resolution spectra have a 1.6 km s^{-1} channel spacing and 280 km s^{-1} bandwidth.

MWC 349 A (α_{J2000} = 20^{h}30^{m}45^s.54, δ_{J2000} = 40°39′36.8″) was observed over an hour angle range from −6 h to +7 h. The series of 20 min integrations were interspersed with observations of the nearby phase calibrator J2005+403 and by pointing and focus measurements. At the middle of the run and immediately before and after it, deep integrations were made on strong point sources for the calibration of the complex instrumental bandpass. The sources 3C 273, 3C 454.3, and 3C 84 were each observed for 2−3 h. A continuum flux density of 1.71 Jy at 232 GHz was adopted for MWC 349 A based on a broadband 1.3 mm measurement (Altenhoff et al. 1994).

The continuum of MWC 349 A is strong enough for self-calibration of the phases. Line-free sections were selected from the low-resolution subband data at each frequency for self-calibration. In this way, the residual phases of the line channels measure the positional offset with respect to the continuum centroid of the source. The statistical errors of the bandpass calibration was ∼1.0° for the longer baselines. No variations of the shape of the bandpass stronger than the measurement accuracy were detected during the run.

After subtracting the continuum in the merged uv tables, we derived the positional offsets and their errors for each spectral channel. These errors are on the order of 2 milliarcseconds (mas) for the channels where the H30α line is stronger than 5 Jy and larger (∼5 mas) for the line wings where the target source dominates the phase noise rather than the bandpass calibration.

3. Results

Figure 1 shows the observed line profile of the H30α line. The lower panel shows the two strong maser spikes and the upper panel the detail of the high-velocity line wings arising from the ionized wind that flows outward (Martín-Pintado et al. 1994).

Figure 2 shows the relative positions of the centroid emission of the H30α line as a function of the radial velocity. The centroids show a very complex distribution, revealing for the first time not only the east-west velocity gradient that is expected for a rotating disk, but the north-south velocity gradients arising from the region where the ionized bipolar outflow arises. There is systematic linear progression of the radial velocities between the maser spikes shown as blue and red circles in Fig. 2, which indicates that this part of the line profile originates in a nearly edge-on rotating disk. The observed velocity gradient and the separation between the two maser spikes (48 mas, 58 AU) are consistent within errors with other measurements. The disk position angle derived from a linear fit to our data, 100.7 ± 0.7 degrees, is also consistent with that measured in other wavelenghts (Planesas et al. 1992; Danchi et al. 2001; Weintroub et al. 2008).

The measured centroid positions for the line wings with radial velocities outside the range between the two masers spikes are dominated by two loops around them (red and blue circles). For the most extreme velocities in the line wings, we measure strong velocity gradients perpendicular to the disk, redshifted to the north and blueshifted to the south, as expected from a bipolar outflow. Furthermore, for the blueshifted emission, the velocity

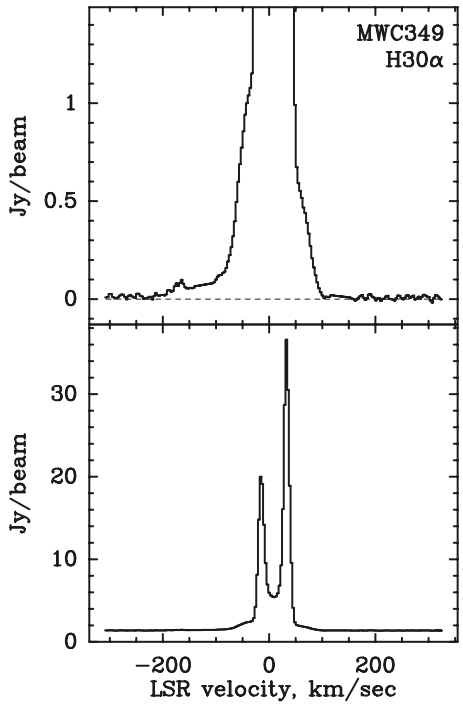

Fig. 1. Line profile of the H30α line toward MWC 349 A. *The lower panel* shows the two strong maser spikes superimposed on the broad asymmetric line wings arising from the the ionized outflow shown in detail in *the upper panel*. The weak feature at ≈−160 km s^{-1} corresponds to emission from heavier atoms such as Helium.

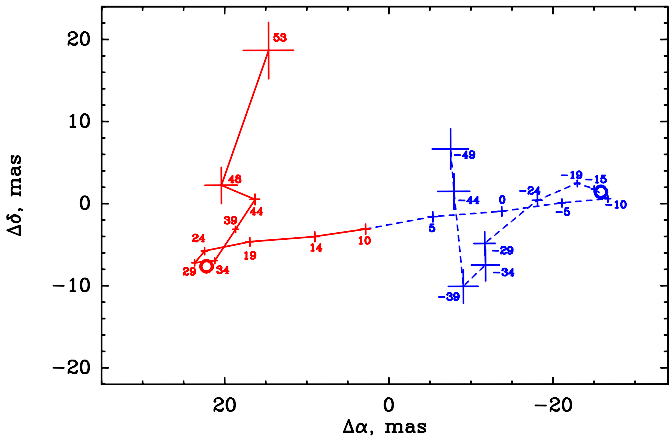

Fig. 2. Map of the relative positions of the H30α centroid emission in MWC 349 A for the velocity range between −49 km s^{-1} and 53 km s^{-1}. The positions of the line channels are shown as crosses labeled by their LSR velocities with the blueshifted and redshifted velocities shown as dashed blue and solid red lines respectively. Maser spikes peak are shown as blue and red circles. Errors are shown by horizontal and vertical bars. The offsets are in milliarcseconds (mas) relative to the continuum centroid.

gradient reverses its direction. As we will discuss in the next sections, this is owing to the wide opening angle of the outflow and its orientation in the sky.

4. Interpretation of the H30α centroid maps. Constraints on the disk and outflow kinematics

The interpretation of the relative centroid maser positions when the emission is un-resolved by the beam is not straightforward

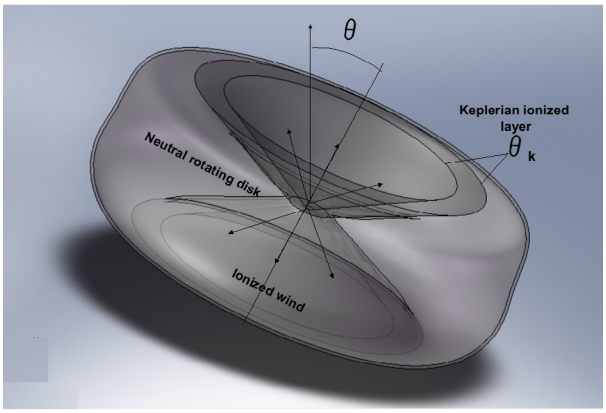

Fig. 3. Sketch of the disk-outflow geometry used in our 3D non-LTE modeling to predict the relative positions of the H30α centroid emission shown in Figs. 4 and 5.

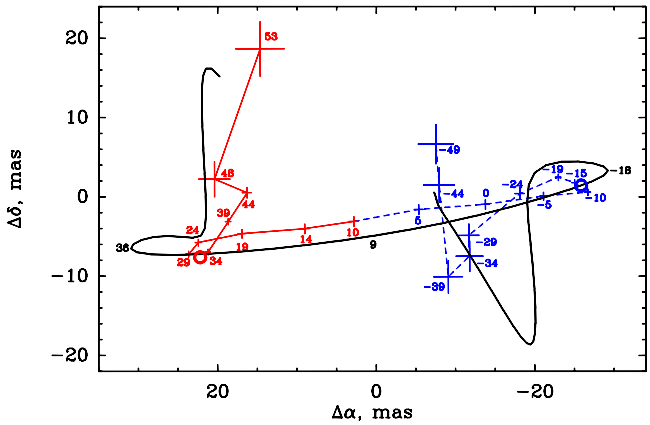

Fig. 4. Model prediction for the relative centroid positions of the H30α emission superimposed (as blue and red thin lines) on the observed data for MWC 349. The radial velocities are as in Fig. 2.

(Weintroub et al. 2008). This is even more complex for the recombination-line masers because they arise simultaneously with the free-free continuum emission. Fortunately, the morphology and the electron density and temperature distribution in MWC 349 A can be very well constrained by the free-free continuum emission. Three-dimensional (3D)-radiative transfer models of the free-free emission predict the continuum spectrum for the whole frequency range (Martín-Pintado 2002) and the continuum bipolar morphology (Martín-Pintado et al. 1993; Tafoya et al. 2004). A sketch of the geometry of the model that best fits the continuum morphology is shown in Fig. 3. The model is composed of a neutral disk that confines the ionized bi-conical outflow with its axis nearly perpendicular to the line of sight. The opening angle of the ionized wind is 57°, and its electron density varies like $r^{-2.14}\exp(\theta/\theta_0)$, where r is the distance to the star and θ is the angle from the cone axis. We took θ_0 to be 17°, and an electron temperature of 12 000 K. The density in the neutral disk and its ionized layer (θ_K in Fig. 3) also varies with radius like $r^{-2.14}$, reaching low densities at relatively small distances from the star.

We used this morphology, density, and temperature structure to predict the H30α positional centroids in Figs. 4 and 5 using our non-LTE 3D radiative transfer model (Martín-Pintado 2002) for the simplest kinematics expected for the disk and the outflow. The kinematics in the model is composed by two velocity components: a) an outflow with radial expansion at a constant velocity of 70 km s^{-1} within the cones and b) a Keplerian rotation for a thin ionized layer (θ_K in Fig. 3) of thickness 6.5° on the surface of the neutral disk (Martín-Pintado et al. 1994) with an electron temperature of 10 000 K. Our simple model has a velocity discontinuity at the ionized disk layer (θ_K in Fig. 3).

Our model is not very sensitive to the electron temperatures from 9000 K to 13 000 K. The terminal velocity of the wind is constrained by the line profile to within 10 km s^{-1}. The inclination of the disk can be constrained to 3–9°. The ionized Keplerain layer (θ_K) must be between 4.5° and 15°.

The predicted centroid positions as a function of radial velocity were obtained as intensity-weighted average position from the H30α line cubes that were generated by the model with a pixel size of 2 mas and a velocity resolution of 3 km s^{-1}. The line profiles predicted by our model for the H30α line show that the two maser spikes (Fig. 1) arising from the disk surface and the asymmetric line wings arising from the wind agree well with observational trends (see e.g. Martín-Pintado 2002). Figure 4 shows as black thick line the best (by eye) predicted centroid distribution superimposed on the observed data. The overall predicted centroid distribution matches the observed trends for the whole radial velocity range very well, including the outflow and the disk kinematics. Indeed, there is an excellent agreement particularly for the blueshifted gas located south of the disk, and even the direction change of the velocity gradient from north-south to south-north is reproduced with similar spatial distribution.

4.1. Disk kinematics. Keplerian rotation

The precise kinematics of the disk is at present unclear. Different central masses are required depending on the quantum number of the observed recombination-line (Thum et al. 1992; Martín-Pintado 2002; Weintroub et al. 2008). The central mass is poorly constrained in our model by the centroid map in Fig. 4, but it is very sensitive to the predicted line profiles (Fig. 1). The centroid map can be fitted with central masses of 30–60 $M_\odot$. However, the predicted velocity separation of the two maser spikes changes from the observed ~48 km s^{-1} for a central mass of ~50 $M_\odot$ to ~30 km s^{-1} for ~30 $M_\odot$, which is inconsistent with the observations. Because the predicted line profiles are also sensitive to the departure coefficients, the ~30 $M_\odot$ central mass should be preferred.

The loops around the maser peaks are caused by the inclination of the disk with respect to the line of sight. The height of the loop depends on the inclination angle. Smaller inclination angles decrease the loop height, disappearing for an edge-on disk owing to the north-south symmetry. Decreasing the disk inclination will require an increase of the outflow terminal velocity to fit the velocity gradients perpendicular to the disk. However, terminal velocity that is too high would not fit the line profiles. Our model also roughly reproduces the height of the loops.

4.2. Hydrodynamic photoevaporating disks

The origin of the outflow is also unknown. Let us consider the analytic photoevaporating disk model (Hollenbach et al. 1994), in which photoevaporation occurs at radii larger than the gravitational radius, R_G. For a 30 $M_\odot$ star, $R_G \sim 150$ AU. No reasonable choice of the input parameters can reproduce the observed centroid distribution. The thick black line in Fig. 5 shows the centroid map predicted by the model. The predicted north-south

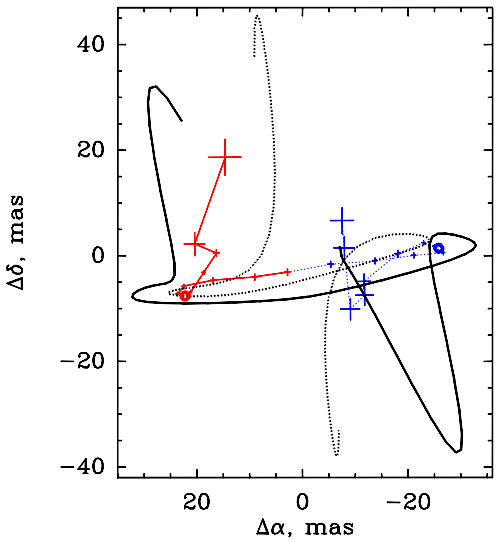

Fig. 5. Predictions for the relative centroid positions of the H30α emissions derived for two different kinematical models superimposed (as blue and red thin lines) on the observed data for MWC 349. The thick black line shows the results for the case when photoevaporation occurs at a radius larger than the gravitational radius. The dotted black line shows the case when the ionized outflow does not follow the disk rotation. The radial velocities are the same as in Fig. 4.

excursions of the centroid position are much larger than the measured values, which is inconsistent with our observations. It is highly unlikely that the ionized outflow in MWC 349 A is produced as described by the analytic hydrodynamic models. However, hydrodynamic simulations of photoevaporating disks around T Tauri stars by (Font et al. 2004) show that the outflow can be launched at radii smaller that R_G by a factor of 3, i.e., ~50 AU. Similar launching radii, ~40 AU, are also obtained from the models of photoevaporation of disks around massive stars (Yorke & Welz 1996). These values better agree with our observations than the analytic models, but they are at least a factor of two larger than those of less than 25 AU, measured by the loop separations in our data in Fig. 2.

4.3. Outflow rotation and acceleration

Measuring the outflow rotation can provide fundamental information on the origin of the outflow. So far, the results obtained from recombination-lines at cm wavelengths have been contradictory. Our best fit to the centroid map is obtained with the wind rotating in the same ways as the disk. This is clearly illustrated in Fig. 5 where we show as a dotted black line our model predictions for the case that the outflowing gas does not participate in the disk rotation. In this case, because the outflow is symmetric, the north-south excursions of the centroid emission arising from the outflow are just along the symmetry axis, near $\Delta\alpha \sim 0$ in Fig. 5. This is completely inconsistent with the observations, suggesting that the outflow is likely launched from the disk, which conserves its angular momentum.

We used a very simple kinematic model to describe the ionized gas outflowing from the disk. We assumed that the wind reaches its terminal velocity just at the disk-wind layer. The good agreement of our model predictions with the observations would indicate that the acceleration of the outflow must occur in a thin layer close to the disk surface. This seems to rule out the possibility that the outflow is launched from the disk as expected in the photoevaporation models. Furthermore, there is also an excellent agreement between the predicted and the measured spatial location (close to the loops) where the outflow seems to be launched, at a radius of ≤20 mas (≤24 AU). Because the loops already trace the launching region, we conclude that the launching of the outflow likely occurs very close to the rotating disk at radii of less than 24 AU.

4.4. The origin of the ionized outflow in MWC 349

The coupling between the disk kinematics and the outflow and the fast acceleration suggest that magnetic wind models might explain the outflow-disk properties observed in MWC 349 A. Magnetic wind models can be divided into two classes: X-winds (Shu et al. 1994) and disk wind models (Blandford & Payne 1982). While in X-wind models the launching of the outflow occurs very close to the star, the disk wind model extends the launching radius farther away from the star to several AU, which better agrees with our results. The presence of strong large-scale magnetic fields up to 30 AU (Thum & Morris 1999) also favors the magnetic disk wind model.

Acknowledgements. We thank the Spanish MICINN for the support provided through grants ESP2007-65812-C02-C01 and AYA2010-21697-C05-01, and AstroMadrid (CAM S2009/ESP-1496). We are grateful to Roberto Neri for advice with the data reduction, Josefina Torres for providing Fig. 3 and the referee, Vladimir Strelnitski, for helpful comments and suggestions.

References

Altenhoff, W. J., Thum, C., & Wendker, H. J. 1994, A&A, 281, 161
Blandford, R. D., & Payne, D. G. 1982, MNRAS, 199, 883
Churchwell, E. 1990, A&ARv, 2, 79
Danchi, W. C., Tuthill, P. G., & Monnier, J. D. 2001, ApJ, 562, 440
Font, A. S., McCarthy, I. G., Johnstone, D., & Ballantyne, D. R. 2004, ApJ, 607, 890
Hollenbach, D., Johnstone, D., Lizano, S., & Shu, F. 1994, ApJ, 428, 654
Jaffe, D. T., & Martín-Pintado, J. 1999, ApJ, 520, 162
Jiménez-Serra, I., Martín-Pintado, J., Rodríguez-Franco, A., et al. 2007, ApJ, 661, L187
Martín-Pintado, J. 2002, in Cosmic Masers: From Proto-Stars to Black Holes, ed. V. Mineese, & M. Reid (San Francisco, CA: ASP), IAU Symp., 206, 226
Martín-Pintado, J., Bachiller, R., Thum, C., & Walmsley, M. 1989, A&A, 215, L13
Martín-Pintado, J., Gaume, R., Bachiller, R., Johnston, K., & Planesas, P. 1993, ApJ, 418, L79
Martín-Pintado, J., Neri, R., Thum, C., Planesas, P., & Bachiller, R. 1994, A&A, 286, 890
Olnon, F. M. 1975, A&A, 39, 217
Planesas, P., Martín-Pintado, J., & Serabyn, E. 1992, ApJ, 386, L23
Ponomarev, V. O., Smith, H. A., & Strelnitski, V. S. 1994, ApJ, 424, 976
Rodriguez, L. F., & Bastian, T. S. 1994, ApJ, 428, 324
Strelnitski, V., Haas, M. R., Smith, H. A., et al. 1996, Science, 272, 1459
Shu, F., Najita, J., Ostriker, E., et al. 1994, ApJ, 429, 781
Tafoya, D., Gómez, Y., & Rodríguez, L. F. 2004, ApJ, 610, 827
Thum, C., & Morris, D. 1999, A&A, 344, 923
Thum, C., Martín-Pintado, J., & Bachiller, R. 1992, A&A, 256, 507
Thum, C., Matthews, H. E., Harris, A. I., et al. 1994, A&A, 288, L25
Thum, C., Martin-Pintado, J., Quirrenbach, A., & Matthews, H. E. 1998, A&A, 333, L63
Weintroub, J., Moran, J. M., Wilner, D. J., et al. 2008, ApJ, 677, 1140
Yorke, H. W., & Welz, A. 1996, A&A, 315, 555